Local temperature measurements in supercritical counterflow in liquid helium II

Paul E. Dimotakis
California Institute of Technology, Pasadena, California 91109

James E. Broadwell
TRW Systems Group, Redondo Beach, California 90278
and
California Institute of Technology, Pasadena, California 91109

(Received 6 February 1973)

In order to investigate the validity of appending the Gorter–Mellink friction term to the equations of motion of liquid helium, the temperature was measured along the axis of a channel carrying a supercritical heat current. A single thermomenter on a traversing assembly was used permitting local measurements both in the interior of the channel and in the jet formed in the free fluid. The temperature gradient in the interior of the channel is found to be in agreement with the Gorter–Mellink law up to the lambda point, but goes to zero within a channel radius, in the free jet. The Gorter–Mellink $A(T)$ was also measured up to the lambda point. A much stronger divergence is found as T_λ is approached than was indicated by previous measurements.

I. INTRODUCTION

In the absence of dissipative mechanisms, the equations of motion for liquid helium II allow an isothermal transport of heat. The heat flux, in the form of entropy of the normal fluid, is then given by

$$\mathbf{q}=\rho s T \mathbf{v}_n,$$

where ρ is the fluid density, s is the entropy per unit mass, T is the absolute temperature, and $\mathbf{v}_n$ is the velocity of the normal fluid. It has long been known, however, that a temperature difference appears between the ends of a long channel which, for small heat fluxes, is found to be proportional to the length of the channel and the heat flux, i.e.,

$$\Delta T=-laq, \tag{1a}$$

where l is the length of the channel, a is a coefficient which depends on temperature and the geometry, and q is the heat flux.

It was possible to account for this temperature difference by assigning a viscosity to the normal fluid. The coefficient a is then given by

$$a=G\eta_n/(\rho s)^2 T,$$

where G is a constant depending on the cross section of the channel (e.g., $G=8/R^2$ for a circular cross section of radius R) and η_n is the viscosity of the normal fluid.

At a certain critical value of q, however, one observes a new dependence of the temperature difference on the heat flux, which for values of q greater than this critical value, is empirically given by

$$\Delta T=-l(aq+bq^3), \tag{1b}$$

where l is the length of the channel.

To account for this cubic dependence of the temperature gradient on the heat flux, in 1949 Gorter and Mellink postulated a frictional force between the two fluids proportional to the third power of the relative velocity.[1] In particular,

$$\mathbf{F}_{sn}=A\rho_n\rho_s w^2\mathbf{w}, \tag{2}$$

where

$$\mathbf{w}=\mathbf{v}_n-\mathbf{v}_s$$

is the difference between the velocity of the normal fluid and the superfluid, respectively. The coefficient A is a universal function of temperature, which has been measured by Vinen.[2] In terms of this mutual friction, the coefficient b is then given by

$$b(T)=A(T)\rho_n/s(\rho_s s T)^3. \tag{3}$$

This coefficient seems to account quite successfully for the observed temperature differences in supercritical counterflow in wide channels. The present work was undertaken to investigate whether this is also a detailed description of the local temperature gradient in a channel and whether the temperature gradients are observed in situations where a heat flux is maintained in the absence of walls.

It was observed by Kapitza[3] that a well-defined jet emerges from the mouth of a counterflow channel that persists for many channel diameters in the free fluid without appreciable spreading. The two-fluid model would identify the effluent with the heat-convecting normal fluid which separates at the channel exit like a classical fluid. In this experiment this was verified by observing the deflection of the free surface of the liquid over the opening of a vertical channel (see Fig. 1). This arrangement creates a well-defined counterflow in the absence of any walls. The temperature along the axis of the channel, both inside and in the jet, was measured by means of a single thermometer mounted on a traversing assembly. This was done at various temperatures and counterflow heat fluxes for two different channels.

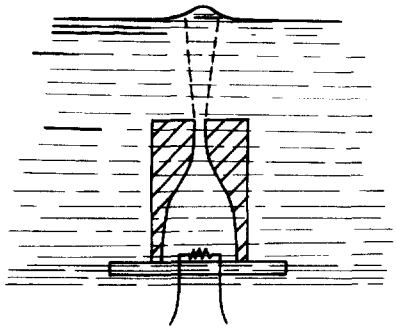

FIG. 1. Free surface deflection by counterflow jet.

II. THE APPARATUS

A. Geometry

Two different flow channels were used (Figs. 2 and 3). Machined out of Plexiglas, they were shaped in such a way as to confine the region of high relative velocities and resulting temperature gradients to a small part of the channel away from the heaters. The heater, in each channel, was constructed with 0.013 cm (0.005 in.) Evanohm wire potted in Wood's metal to insure uniform distribution of heat at the bottom of the channel. The thickness of the channel walls kept heat losses through heat conduction under 1% of the total heat input.

B. Sensors

The bath temperature during the measurement was monitored and recorded by sensing the vapor pressure at the top of the cryostat with a 100-mm Hg full-scale barocel transducer. Bath temperature could be set and maintained to within limits that depended on the heat input to the channel heater, with a condom pressure regulator[4]; a variation of the Walker-type regulator. The temperature versus position along the channel axis was sensed by a carbon thermometer motorized with a variable speed, reversible direct current motor. This was enclosed in the cryostat and situated at the top at room temperature. The shaft of this motor wound and unwound a nylon thread from which the traversing thermometer assembly was suspended. An optimum volume of approximately 1.5×10^{-5} cm^3 was selected for the thermometer tip as a compromise between signal-to-noise ratio which decreased with decreasing size and obstruction to the flow which had to be minimized. It was shaped under a microscope to resemble a cube, approximately 0.025 cm on the side. Two 0.00254 cm (0.001-in.) enameled copper wires whose insulation was sanded off the ends were bonded on opposite faces of the cube with conducting silver paint. These wires were threaded through a 3-mm glass tube drawn to a 0.025-cm capillary, 7.5 cm long and provided the mechanical support and electrical connections to the sensor. (See Fig. 4).

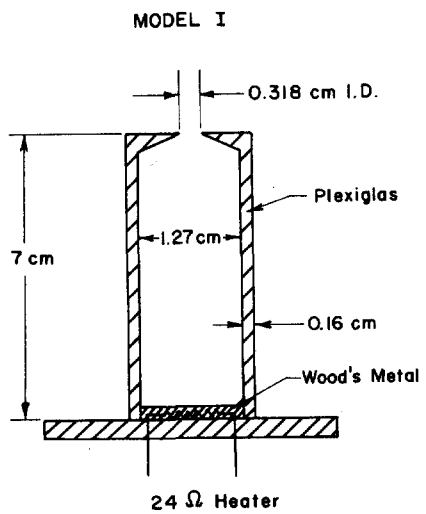

FIG. 2. Orifice counterflow channel.

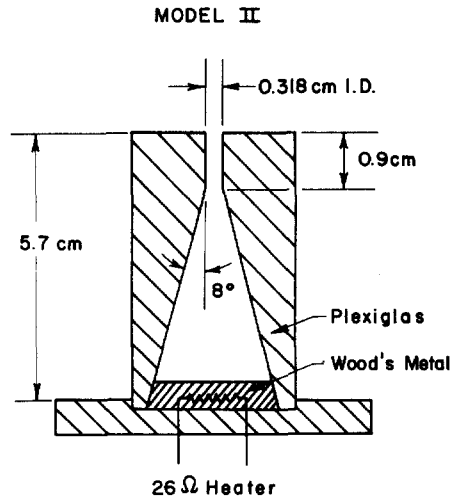

FIG. 3. Constant area counterflow channel.

The glass tube was fitted to a stainless steel thin-walled tube inside a soft iron tube, and moved inside a stationary Plexiglas tube with a 7.6-cm-long coil wound on the outside using 0.025-cm (0.010-in.) magnet wire. The inductance of this coil, a function of the position of the soft iron core, was sensed as a means of measuring the position of the thermometer. The whole assembly could be aligned with the channel axis by means of two sets of three set-screws 120° apart. (See Fig. 5.)

C. Instrumentation and Calibrations

The 100-mm Hg full-scale barocel transducer was coupled to a 1014 barocel electronic manometer whose 0.0- to 10.0-V full-scale linear output was multiplexed by means of an analog channel selector into a six-digit HP3450A integrating digital voltmeter. (See Fig. 6.) The resistance of the channel thermometer was measured by sensing the resistive voltage drop across the carbon tip with a 1.5-kHz reference current with a Princeton Applied Research HR-8 phase locking amplifier, whose linear output of -10.0 to $+10.0$ V

was also multiplexed into the digital voltmeter. Power dissipation in the sensing element was kept under 10^{-8} W in order to minimize any temperature differences between the carbon tip and the surrounding liquid. Calibration of the thermometer was easily carried out before each run by multiplexing between the barocel electronic manometer and the thermometer amplifier, as the bath temperature was allowed to drift slowly.

The inductance of the position sensing coil was measured on a second-phase locking amplifier by observing the inductive voltage drop across the coil with a 30-kHz reference current. Linearity was better than 0.1% over the traversing range of interest. Calibration was realized by noting the output of the position sensing amplifier versus measurements of the position of the temperature sensing tip with a cathetometer from the outside. The procedure yielded an absolute accuracy of the order of 0.01 cm with respect to the channel exit, as limited by the cathetometer readings through the vessels. Note that possible stretching of the nylon thread did not affect the accuracy of the position measurement, since the sensing is realized at the bottom of the Dewar with a device that is integrally connected to the temperature sensing tip. The output of the position sensing amplified was also multiplexed into the digital voltmeter.

Finally, the voltage drop across a 100-Ω resistor, in series with the channel heater, was also multiplexed as a fourth input into the digital voltmeter. This monitored the power driving the couterflow. The heater current was supplied by a Hewlett–Packard 6201B regulated power supply.

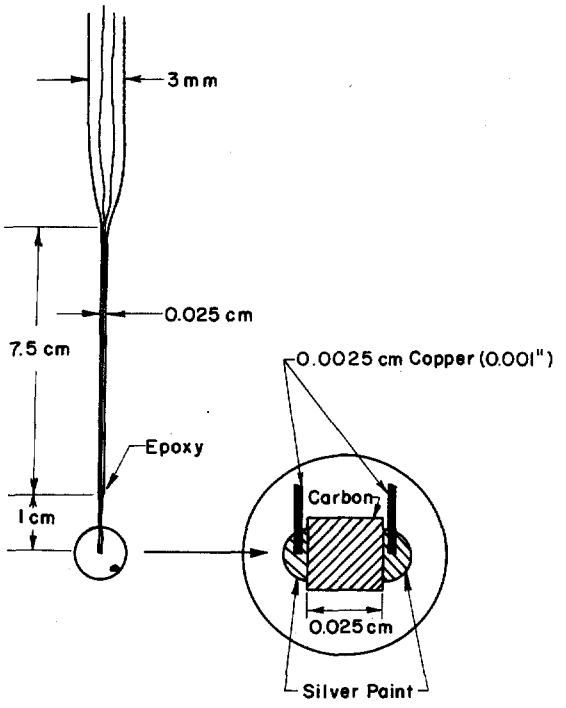

FIG. 4. Temperature sensor.

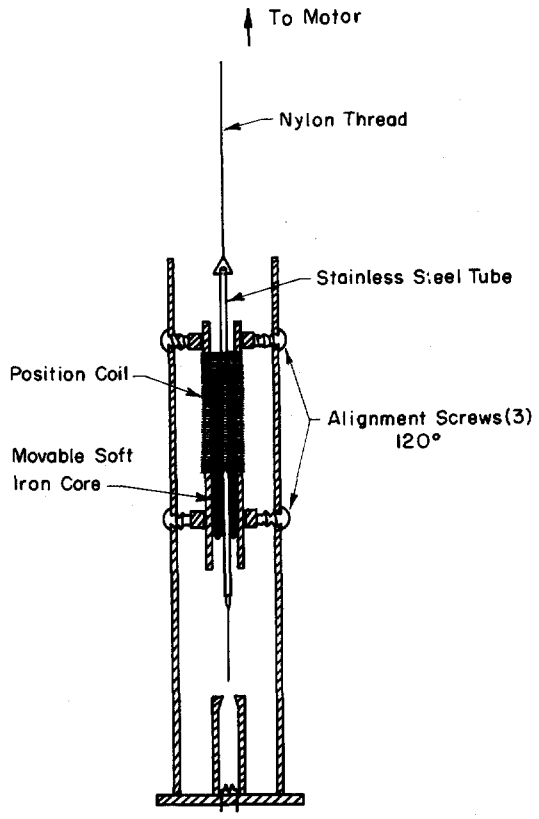

FIG. 5. Thermometer assembly and counterflow channel.

The analog channel selector (Ref. 5, Appendix 1) utilized gold contact, sealed relay switches for both signal and ground to avoid common-mode errors and cross-talk between the channels. The four inputs were selected in sequence by the programming logic and connected to the guarded input of the digital voltmeter. No measurable contact noise or bias originating in the analog channel selector was detectable on the digital voltmeter (1-μV resolution).

The 32-bit output of the digital voltmeter was formatted into four 8-bit characters (bytes) and written on a 9-track, 800 BPI Kennedy 1600/360 incremental tape recorded by a digital data coupler (Ref. 5, Appendix 2). The tape was read on an IBM 360/75 to process the data and plot the results.

An X–Y plotter, connected to the inputs during each run, provided real-time monitoring of the data and an additional check on the computer processed results. A block diagram of the instrumentation package appears in Fig. 6.

III. EXPERIMENTAL PROCEDURE

The bath temperature was set to the desired value by means of the condom regulator and a trial traverse was made using the highest anticipated heat flux, as limited by cavitation[6] at the bottom of the channel, to determine the range of the output of the thermometer amplifier. This output was then calibrated and recorded on tape versus vapor pressure, in a quiescent bath, by

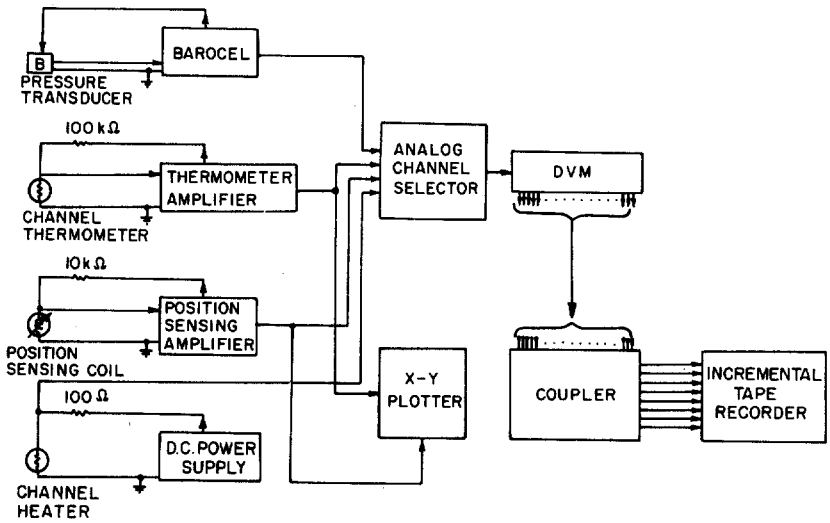

FIG. 6. Instrumentation.

multiplexing between the barocel output and the thermometer amplifier while the bath temperature was allowed to drift to cover the anticipated range. Two traverses, one in each direction, were then made for each value of the heat flux. The voltage outputs from the barocel thermometer amplifier, position amplifier, and heater current sensing resistor (100 Ω) were recorded in sequence (75 msec apart) at sampling intervals ranging from 0.5 to 1 sec depending on the rate of traverse and consistent with the 300 msec integrating times on the phase locking amplifiers, as the thermometer traversed slowly. Finally, the output of the sensing amplifier was calibrated versus position by means of a cathetometer. The data for this calibration were punched on computer cards and processed with the tape. Parabolic least-squares fit were used to express in analytical form the thermometer amplifier versus pressure and position amplifier versus position calibrations. The conversion from vapor pressure to degrees Kelvin was through an Aitken third order interpolation on the National Bureau of Standards 1958 ^{4}He temperature scale. Thus, the bath temperature, the channel temperature, and the heater power could be calculated for each position x of the channel thermometer. At the power levels that were used to drive the counterflow, small fluctuations in the vapor pressure regulating system necessitated computing the difference between the channel temperature and the simultaneous bath temperature. This difference was then added to the average bath temperature during the traverse. Sample data are plotted in Figs. 7–9. The continuous line in Fig. 9 consists of straight line segments connecting 182 data points. The abscissa is scaled in centimeters along the channel axis as measured from the channel exit. Positive values of x correspond to positions in the jet. Negative values of x correspond to the interior of the channel. The ordinate is scaled in degrees Kelvin.

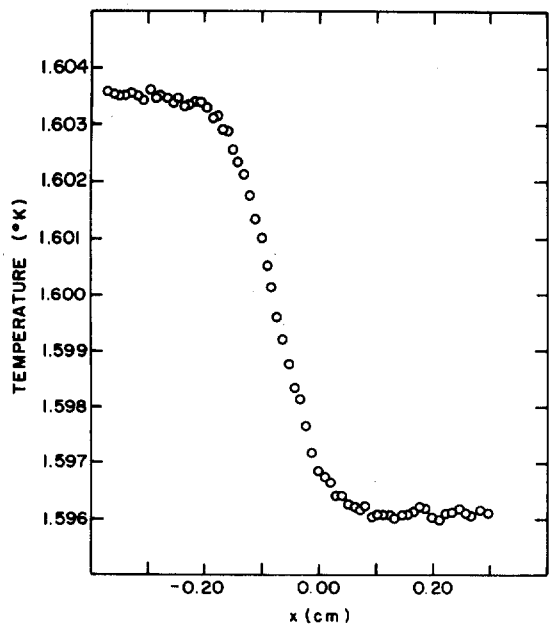

FIG. 7. Model I data, $q=2.66$ W/cm^2.

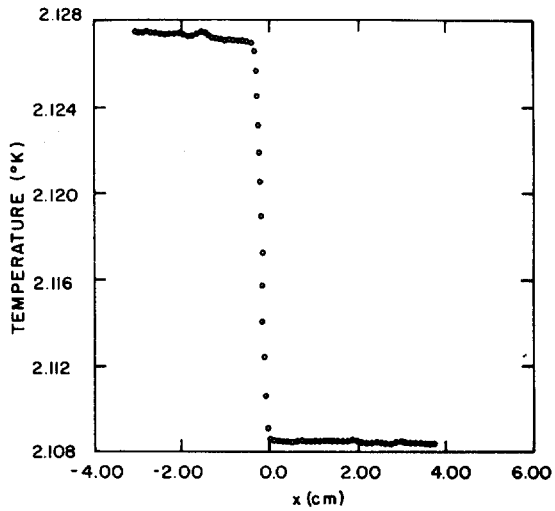

FIG. 8. Model I data, $q=3.52$ W/cm^2.

IV. RESULTS AND DISCUSSION

The quantitative behavior of the temperature field in one-dimensional counterflow with zero mass flux should be described by Eq. (1b). For high heat fluxes this should result in a local temperature gradient given by

$$dT/dx = -b[T(x)]q^3(x), \tag{4}$$

where $b(T)$ is given by Eq. (3).

It should be emphasized that Eq. (4) yields two independent predictions. One is that at any point in a given counterflow channel, held at a fixed temperature, the temperature gradient would be proportional to the cube of the local heat flux, and two, that the constant of proportionality, $b(T)$, is a universal function of temperature.

The apparent "deviations" from the cubic law which are characteristic of experiments that measure temperature differences between the ends of a long tube as a function of the applied heat flux, can be explained in terms of the temperature dependence of $b(T)$. This becomes apparent from the data taken with model II.

Within the constant area section of model II, $q(x)$ is constant and equal to the value at the exit ($x=0$). Therefore, if

$$q^* = q(0),$$

we have

$$(q^{*3})^{-1}(dT/dx) = -b(T).$$

If this is indeed a local law, we should be able to observe a change in $b(T)$ within the temperature interval that appears between the ends of the constant area section of model II. A close look at Fig. 9 shows a

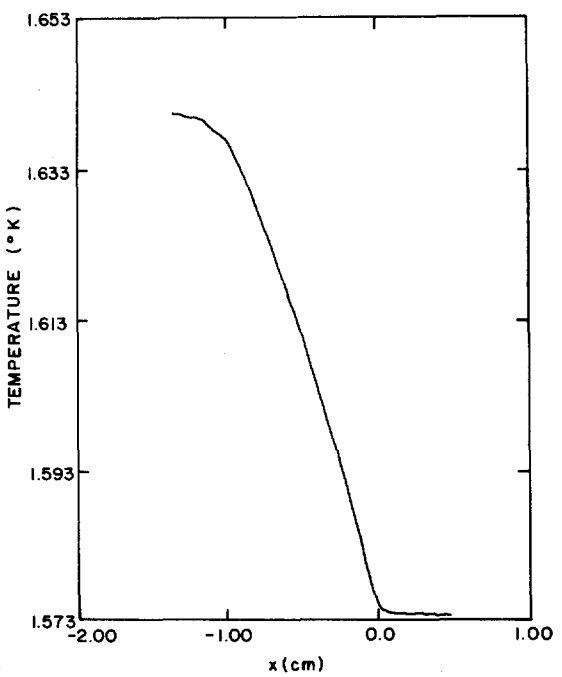

FIG. 9. Model II data, $q=2.67$ W/cm².

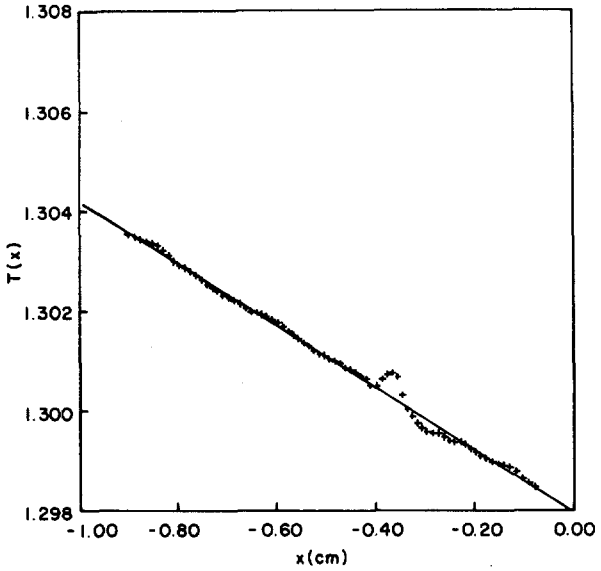

FIG. 10. Model II data, $q=0.46$ W/cm².

systematic change in the slope dT/dx as a function of temperature. To check this, measurements in the constant area section of model II were fitted with a quadratic to obtain both the derivative dT/dx and the change in the derivative which gives $db(T)/dT$. Three such fits are plotted from data at 1.3°, 1.4°, and 1.5°K in Figs. 10–12. From the quadratic fit, $b(T)$ is then calculated at sixteen points as a function of T within the temperature interval covered in each run. The results are plotted in Fig. 13. It can be seen that the measurements are consistent with each other, inasmuch as the smooth line that joins the three runs is consistent with the estimates of $b(T)$ for the three intervals. It should be emphasized that in this way both $b(T)$ and $db(T)/dT$ are determined in a constant area channel 0.9 cm long. The inconsistency in the curvature of the three estimates is a consequence of the quadratic fit. The cubic fit which could have provided the correct curvature would have required a longer constant area section.

These data and data from model I are compared to those of Vinen[2] and Broadwell and Liepmann[6] in Fig. 14. It can be seen that the data from model II and those of Vinen agree very well with each other. It can also be seen that $b(T)$ as deduced from the data from model I is systematically lower than the measurements of Vinen and those from model II. In the case of model I, $b(T)$ was calculated by dividing $(dT/dx)_{max}$ for each traverse, by q^{*3}. As can be seen from Fig. 7, the maximum gradient does not occur at the orifice but approximately half a millimeter inside the channel where the heat flux is probably a little smaller. The differences of the order of 10% which arise are probably attributable to this reason.

The data from model I, however, can be used to check the predictions of the Gorter–Mellink law in a different manner. To do this we must first show that

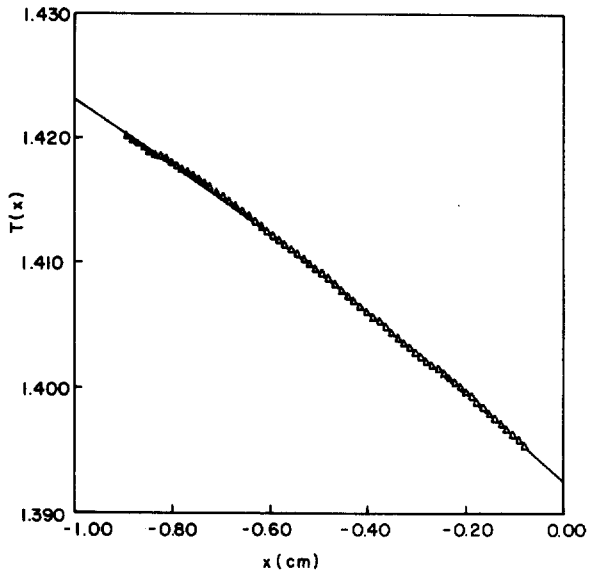

FIG. 11. Model II data, $q=1.14$ W/cm².

the scaled temperature profile,

$$\theta(x)=[T(x)-T_\infty]/\Delta T,$$

where ΔT is the difference in temperature between the interior and the exterior, and T_∞ the bath temperature, is independent of T_∞ and q^*.

Equation (4) can be separated to give

$$\frac{1}{q^{*3}}\frac{dT}{b(T)}=-\left(\frac{q(x)}{q^*}\right)^3 dx. \tag{5}$$

Thus, we can integrate from a station x_1 to an arbitrary x to obtain

$$\frac{1}{q^{*3}}\int_{T(x_1)}^{T(x)}\frac{dT'}{b(T')}=-\int_{x_1}^{x}\left(\frac{q(x)}{q^*}\right)^3 dx. \tag{6}$$

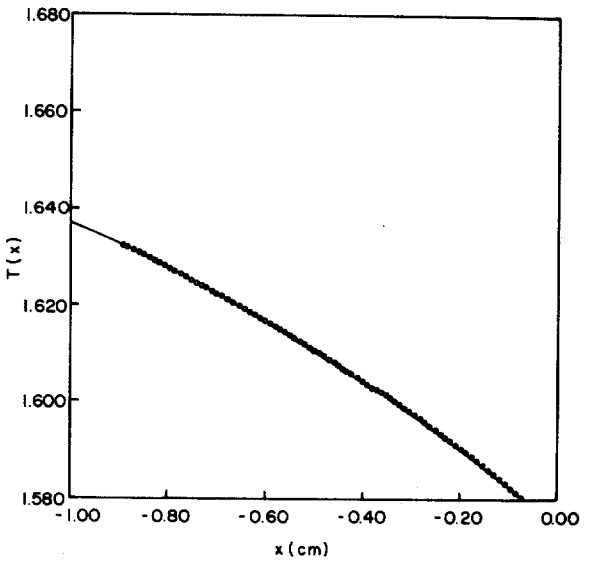

FIG. 12. Model II data, $q=2.67$ W/cm².

By the mean value theorem,

$$\frac{1}{q^{*3}}\int_{T(x_1)}^{T(x)}\frac{dT'}{b(T')}\simeq[q^{*3}b(T)]^{-1}\int_{T(x_1)}^{T(x)}dT'$$

$$=\frac{T(x)-T(x_1)}{q^{*3}b(T)},$$

where

$$T(x_1)<T<T(x).$$

We now use the experimental observation that the temperature gradient vanishes in the jet within a radius from the exit. If x_1 is a station in the jet where the temperature gradient is effectively zero, and we integrate to a station x_2 in the interior of the channel,

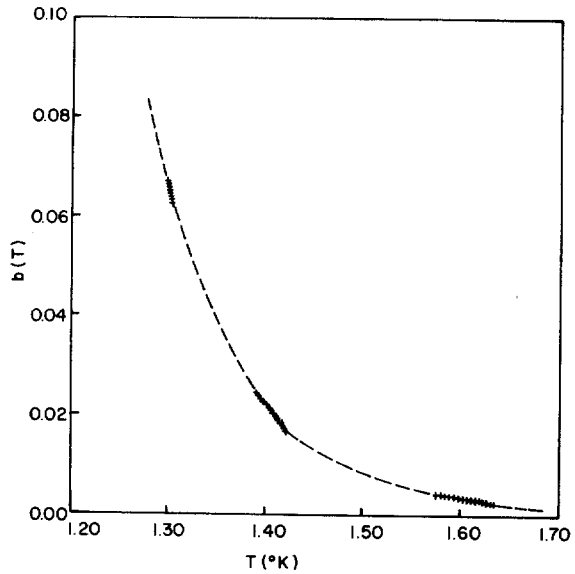

FIG. 13. $b(T)$ calculated from three runs of model II.

we obtain

$$\frac{T(x_2)-T_\infty}{q^{*3}b(T)}=\frac{\Delta T}{q^{*3}b(T)}=\int_{x_2}^{x_1}\left(\frac{q(x)}{q^*}\right)^3 dx.$$

The integral on the right-hand side is a constant with units of length, scaling the transition region in the temperature profile between the channel interior and the channel exterior. Let

$$\int_{x_2}^{x_1}\left(\frac{q(x)}{q^*}\right)^3 dx=l.$$

Therefore,

$$\Delta T/q^{*3}b(T)=l \tag{7}$$

and

$$\frac{T(x)-T_\infty}{q^{*3}b(T)}\propto\frac{T(x)-T_\infty}{\Delta T}=\theta(x).$$

To check this, $\theta(x)$ was plotted versus x, for sample runs from model I, on Fig. 15. It can be seen that the similarity that is predicted by the equations of motion is borne out by the experiment. We can also use Eq. (7) to check the dependence of ΔT on q^*. All the

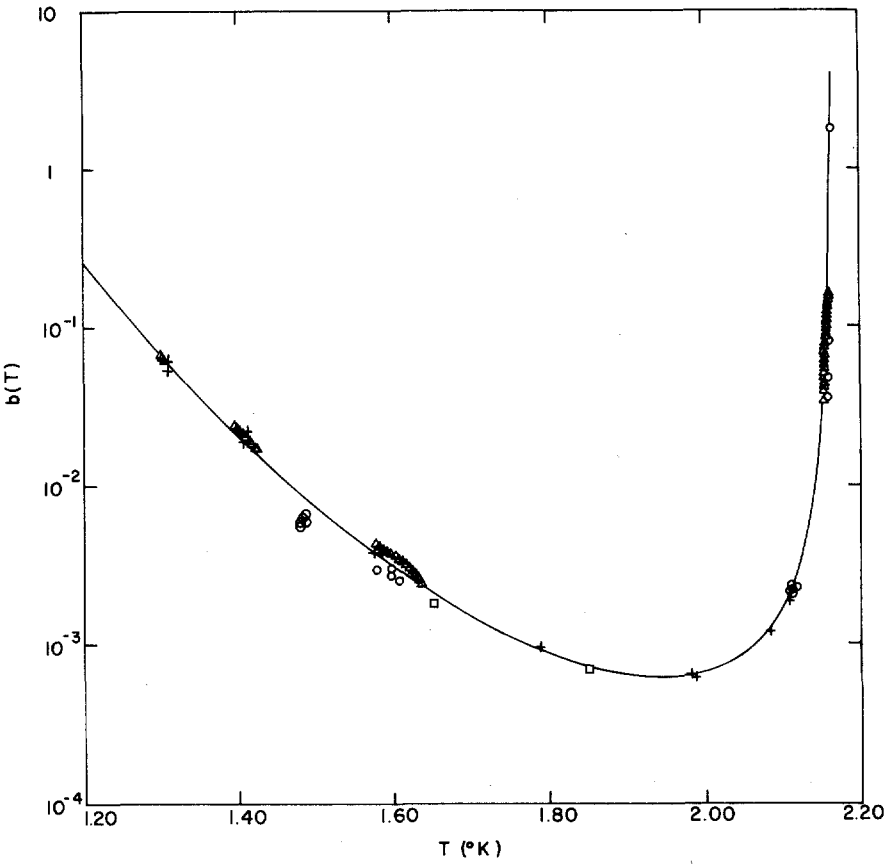

FIG. 14. The universal function $b(T)$. ○ model I data, △ model II data, + Vinen[2] data, □ Broadwell and Liepmann[7] data.

data from model I, except one traverse at 2.165°K (see Fig. 14), for which the change in $b(T)$ even within the small ΔT was large, are plotted in Fig. 16. The data have been grouped such that the temperature for each group, rounded off to three significant figures, is the same. This grouping corresponds to the clusters of points that appear in Fig. 14. The constant l of Eq. (17) turns out to be equal to 0.126 cm. The straight line in Fig. 16 is a plot of

$$\Delta T/b(T)=0.126q^{*3}.$$

Error bars are smaller than the size of the symbols. The values of $b(T)$ used to scale the temperature differences are taken from the smooth line on Fig. 14.

The calculation of the Gorter–Mellink constant $A(T)$, from the experimentally determined $b(T)$, on the basis of Eq. (3) involves the use of the thermodynamic functions for liquid helium and the ratio ρ_s/ρ as a function of temperature. Because errors have been found in the available tables in the literature, the values that were used in this calculation are listed in Table I. These values were determined by requiring that the first differences between the entries, divided by the temperature difference, be a smooth function of temperature. The resulting values of $A(T)$ are plotted in Fig. 17. It can be seen that there exists a strongly divergent regime in the neighborhood of the lambda point that could not have been predicted by extrapolating Vinen's measurements.

A plot of $\log A(T)$ versus $\log T$ reveals a power law dependence on T for temperatures less than 2.0°K. It was found that the divergent part near the lambda point could be represented by an exponential divergence. The smooth line on Fig. 17 is a plot of the function

$$\log_{10}A(T)=c_1+c_2\log_{10}T+[c_3/(1-T/T_\lambda)], \quad (8)$$

where a least-squares determination of the three coefficients yielded

$$c_1=1.0999,$$
$$c_2=3.1227,$$
$$c_3=0.0076.$$

The smooth line in Fig. 14 for $b(T)$ was calculated on the basis of Eq. (3) using the values of $A(T)$ as calculated by Eq. (8).

Numerical values for $A(T)$ and $b(T)$ on the basis of Eq. (8) are given in Table I.

Qualitatively, the most striking feature of the temperature measurements in this experiment is the absence of a temperature gradient outside the channel, as can be seen from the data in Fig. 7 and 8. In this region, the deviations of the resistance of the traversing thermometer from a constant value are random and reflect the low-frequency noise spectrum that characterized the small carbon thermometer. The gradient that is found in the interior of the channel disappears

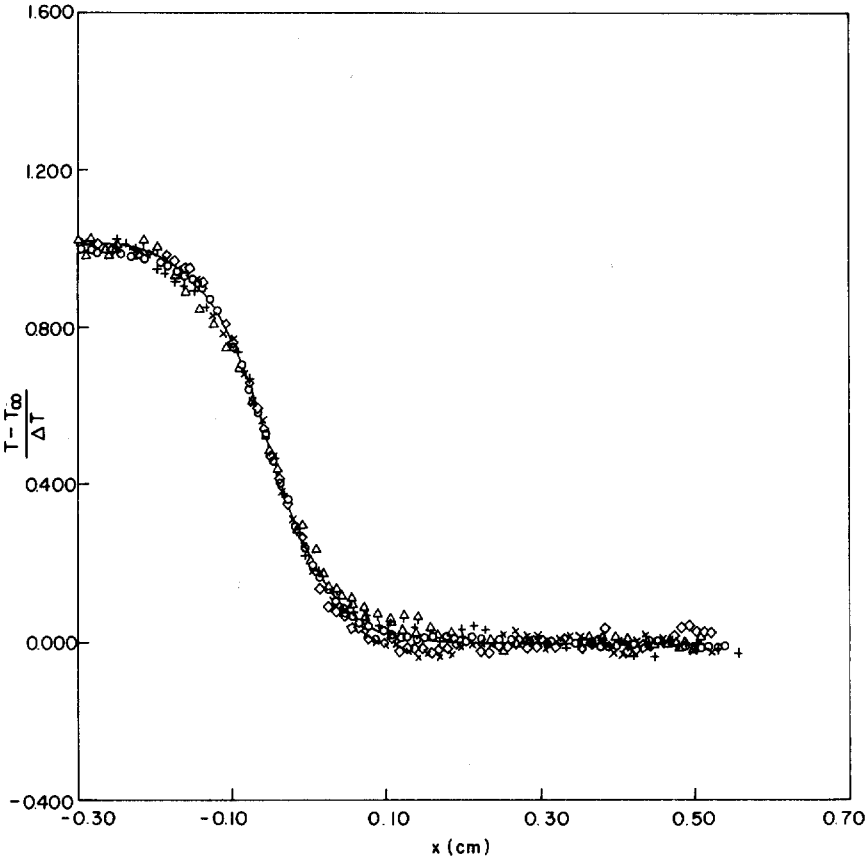

FIG. 15. Model I data similarity.
○ $T_\infty = 1.587$ °K, $q = 3.301$ W/cm².
◇ $T_\infty = 1.595$ °K, $q = 2.637$ W/cm².
△ $T_\infty = 1.560$ °K, $q = 2.866$ W/cm².
△ $T_\infty = 2.153$ °K, $q = 0.8158$ W/cm².
+ $T_\infty = 2.154$ °K, $q = 0.7193$ W/cm².
× $T_\infty = 2.154$ °K, $q = 0.7187$ W/cm².

in the free jet within a channel radius from the channel exit. This fact has to be reconciled with the persistence of the normal fluid jet for several channel diameters into the free fluid. Equation (4), for example, can no longer be valid, since $q(x)$ is not appreciably smaller in the jet, a diameter away from the exit. Unfortunately, the complexity of the equations of motion and the uncertainty concerning the higher-order terms in the velocity do not allow a rigorous theoretical clarification of this point. It is the authors' opinion, at this time, that additional measurements of other field

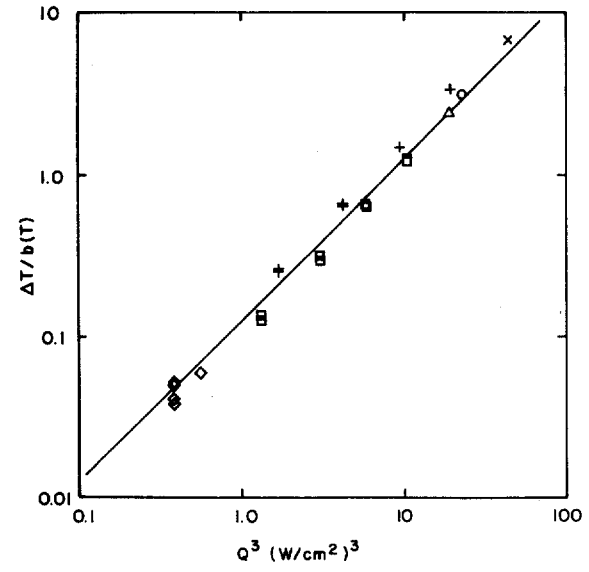

FIG. 16. Model I heat transfer data. □ 1.48 °K, ○ 1.58 °K, △ 1.60 °K, + 2.11 °K, × 2.12 °K, ◇ 2.16 °K. The straight line is a plot of $\Delta T/q^3 b(T) = 0.126$ cm.

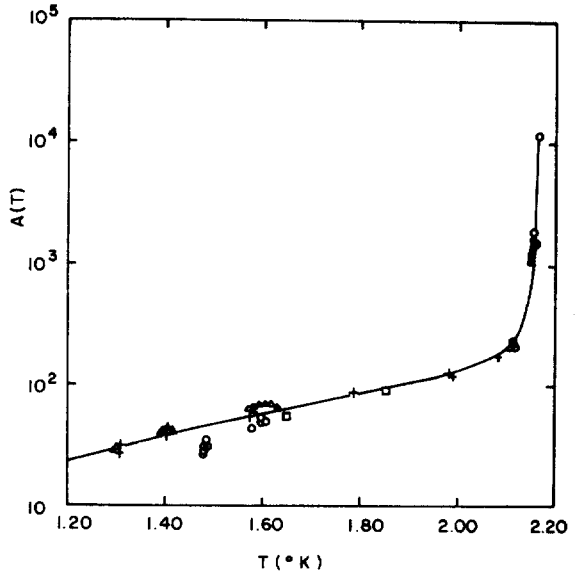

FIG. 17. The Gorter–Mellink $A(T)$. ○ model I data, △ model II data, + Vinen[2] data, □ Broadwell and Liepmann[7] data. Smooth line is a plot of $\log_{10}A = 1.0999 + 3.1227 \log_{10}T + 0.0076/(1 - T/T_\lambda)$.

variables, such as the velocities and chemical potential are required. Experimental work is presently in progress along these lines. Local measurements can clarify not only the analytical description of the mutual friction but also shed light into the dissipative mechanism that is phenomenologically described by the cubic law. It should be noted, for example, that the temperature gradient does extend a little (a channel radius) into the free fluid. An interesting conclusion can be drawn from this observation.

Current theories of the mutual friction[7] view the dissipative mechanism as an interaction between the quantized vortex lines, that render the superfluid turbulent, and the elementary excitations that compose the normal fluid. If this turbulent state of the superfluid, however, bears any resemblance to turbulence as observed in classical fluids, we should have observed an inlet length corresponding to the persistence of the potential core of the incoming fluid. Vinen,[8] in fact, considered this idea of an inlet length, on the basis of the build-up times which he measured for the onset of the dissipative mechanism. Reasoning by analogy to classical boundary layer theory, he estimated an inlet length for the process given by the product of the flow velocity and the build-up times. He was forced to conclude from his own data, however, that any length computed on such a basis would be too large. The conclusion that is borne by the present data is that even the notion of an inlet length is inapplicable to the phenomenon; the temperature gradient would have vanished in the interior of the channel and not have extended at all in the jet.

V. CONCLUSION

The small traversing thermometer that was developed for the present experiments permitted local measurements of temperature from which the following conclusions can be drawn. In the interior of the channels the proportionality of the temperature gradient to the cube of the heat flux is found to hold locally. Furthermore, the universality of the constant of proportionality is verified. The Gorter–Mellink constant appears to diverge as T_λ is approached more rapidly than was indicated by measurements in the past. In fact, the empirical formula

$$\log_{10}A(T)=1.10+3.12\log_{10}T+[0.0076/(1-T/T_\lambda)]$$

is found to be a good representation for $A(T)$ in the range of temperatures, 1.3° to 2.16°K, covered in this experiment.

The temperature gradient in the free jet falls to zero within a channel radius of the exit as the temperature approaches the bath temperature. Unfortunately, it is not possible at this point to establish whether or not this behavior is consistent with the equations of motion including the Gorter–Mellink term. The fact, however, that the temperature gradient extends at all into the free fluid suggests that the dissipative mechanism is probably not describable in terms of turbulence in the superfluid.

TABLE I. The Gorter–Mellink constants as a function of temperature.[a]

T	ρ_s/ρ	s	ρ	$A(T)$	$b(T)$
°K		J/g·°K	g/cm³	cm·sec/g	$\frac{°K/cm}{(W/cm^2)^3}$
1.20	0.9721	0.0523	0.1451	2.31(1)	2.58(−1)
1.25	0.9629	0.0672	0.1451	2.63(1)	1.30(−1)
1.30	0.9527	0.0853	0.1451	2.98(1)	6.66(−2)
1.35	0.9392	0.1069	0.1451	3.36(1)	3.65(−2)
1.40	0.9233	0.1320	0.1451	3.78(1)	2.10(−2)
1.45	0.9057	0.1620	0.1451	4.23(1)	1.22(−2)
1.50	0.8842	0.1970	0.1451	4.72(1)	7.39(−3)
1.55	0.8594	0.2378	0.1451	5.26(1)	4.65(−3)
1.60	0.8314	0.2840	0.1451	5.84(1)	3.05(−3)
1.65	0.8000	0.3367	0.1451	6.47(1)	2.08(−3)
1.70	0.7645	0.3959	0.1452	7.15(1)	1.48(−3)
1.75	0.7247	0.4617	0.1452	7.91(1)	1.11(−3)
1.80	0.6804	0.5352	0.1453	8.74(1)	8.78(−4)
1.85	0.6310	0.6170	0.1453	9.67(1)	7.33(−4)
1.90	0.5757	0.7091	0.1454	1.07(2)	6.52(−4)
1.95	0.5138	0.8122	0.1455	1.20(2)	6.31(−4)
2.00	0.4448	0.9290	0.1456	1.37(2)	6.83(−4)
2.05	0.3678	1.0620	0.1457	1.62(2)	8.83(−4)
2.06	0.3510	1.0940	0.1457	1.69(2)	9.53(−4)
2.07	0.3330	1.1240	0.1457	1.77(2)	1.06(−3)
2.08	0.3150	1.1550	0.1458	1.87(2)	1.21(−3)
2.09	0.2960	1.1850	0.1458	2.00(2)	1.42(−3)
2.10	0.2769	1.2150	0.1458	2.16(2)	1.72(−3)
2.11	0.2550	1.2520	0.1458	2.39(2)	2.19(−3)
2.12	0.2318	1.2870	0.1459	2.73(2)	3.03(−3)
2.13	0.2068	1.3220	0.1459	3.30(2)	4.71(−3)
2.14	0.1782	1.3610	0.1460	4.44(2)	9.00(−3)
2.15	0.1442	1.4000	0.1460	7.73 2)	2.71(−2)
2.16	0.1044	1.4420	0.1464	3.31(3)	2.79(−1)

[a] *Note*: Numbers in parentheses indicate powers of ten multiplying entries.

ACKNOWLEDGMENTS

The authors would like to thank Dr. H. A. Notarys for his invaluable advice throughout the course of this experiment and Professor H. W. Liepmann for many illuminating discussions.

The present work was supported by the Sloan Fund of the California Institute of Technology.

[1] C. J. Gorter and J. H. Mellink, Physica (The Hague) **15**, 285 (1949).
[2] W. F. Vinen, Proc. R. Soc. A **240**, 114 (1957).
[3] P. L. Kapitza, J. Phys. USSR **4**, 181 (1941).
[4] H. A. Notarys (private communication).
[5] P. E. Dimotakis, Ph.D. thesis, California Institute of Technology, 1972.
[6] J. E. Broadwell and H. W. Liepmann, Phys. Fluids **12**, 1533 (1969).
[7] W. F. Vinen, Proc. R. Soc. A **242**, 493 (1957).
[8] W. F. Vinen, Proc. R. Soc. A **240**, 128 (1957).